Real-time high-bandwidth mm-wave 5G NR signal transmission with analog radio-over-fiber fronthaul over multi-core fiber

Simon Rommel[1*], Evangelos Grivas[2], Bruno Cimoli[1], Delphin Dodane[3], Alvaro Morales[1], Evangelos Pikasis[2], Jerome Bourderionnet[3], Gilles Feugnet[3], Juliana Barros Carvalho[1], Michail Katsikis[4], Konstantinos Ntontin[4], Dimitrios Kritharidis[4], Izabela Spaleniak[5], Paul Mitchell[5], Mykhaylo Dubov[5] and Idelfonso Tafur Monroy[1]

*Correspondence:
simon.rommel@ieee.org
[1] Institute for Photonic
Integration, Eindhoven
University of Technology,
5600 MB Eindhoven, The
Netherlands
Full list of author information
is available at the end of the
article

Abstract

This article presents an experimental demonstration of a high-capacity millimeter-wave 5G NR signal transmission with analog radio-over-fiber (ARoF) fronthaul over multi-core fiber and full real-time processing. The demonstration validates the core of the blueSPACE fronthaul architecture which combines ARoF fronthaul with space division multiplexing in the optical distribution network to alleviate the fronthaul capacity bottleneck and maintain a centralized radio access network with fully centralized signal processing. The introduction of optical beamforming in the blueSPACE architecture brings true multi-beam transmission and enables full spatial control over the RF signal. The proposed ARoF architecture features a transmitter that generates the ARoF signal and an optical signal carrying a reference local oscillator employed for downconversion at the remote unit from a single RF reference at the central office. A space division multiplexing based radio access network with multi-core fibre allows parallel transport of the uplink ARoF signal and reference local oscillator at the same wavelength over separate cores. A complete description of the real-time signal processing and experimental setup is provided and system performance is evaluated. Transmission of an 800 MHz wide extended 5G NR fronthaul signal over a 7-core fibre is shown with full real-time signal processing, achieving 1.4 Gbit/s with a bit error rate $< 3.8 \times 10^{-3}$ and thus below the limit for hard-decision forward error correction with 7% overhead.

Keywords: 5G, Millimeter waves, Analog radio-over-fiber, Real-time processing

1 Introduction

The imminent introduction of fifth generation mobile networks (5G) is set to drastically alter the architecture and layout of mobile networks to satisfy the continuously rising demand for mobile data and to accommodate a whole range of novel applications with varying requirements. As a result, 5G networks promise Gbit per second class user data rates, much reduced latency and support for extreme user densities [1–3]. In order to support the ambitious key performance indicator (KPI) targets

Rommel *et al. J Wireless Com Network*   (2021) 2021:43

Page 2 of 20

of up to 1000× higher capacity, multi-Gbit/s user data rates, latencies down to 1 ms and up to 100× the number of connected devices, significant changes are required. The changes brought by 5G networks affect all parts of the system, from the core over the radio access network (RAN) to the air interface and user equipment (UE) as well as in the orchestration and management of the network [4, 5]. The introduction of 5G new radio (NR) brings substantial reductions in latency and allows for bandwidths multiple-times larger than in 4G long-term evolution (LTE) networks, especially through the newly introduced millimeter wave (mm-wave) bands in 3GPP frequency range 2 (FR2) [6].

The introduction of mm-waves, on one hand, allows larger over the air capacities through increased available bandwidth and spectrum, but, on the other hand, poses key challenges to the network deployment, as it requires smaller cells and thus a denser network [7, 8]. Such a densified deployment of macro- and pico-cells makes the use of centralized radio access networks (C-RANs) highly attractive, as they allow dynamic reaction to varying user loads and traffic demands through centralization and pooling of signal processing resources. The resulting load on optical distribution networks (ODNs) from the fronthaul required for a highly densified network deployment with the use of very large bandwidths and advanced radio techniques such as beamforming or multiple-input multiple-output (MIMO) transmission however poses major challenges and creates an important bottleneck. The latter is true both on the scale of the overall network, but also for each fronthaul link individually, as current fronthaul technologies such as common public radio interface (CPRI) scale poorly to large bandwidths and multi-sector or MIMO antenna deployments [9].

As the increased spatial control over the radio frequency (RF) signal afforded by MIMO transmission or beamforming is required to achieve the capacity and energy efficiency targets for 5G networks, substantial research activity is focused on improved fronthaul solutions. The main research directions are either to partially re-distribute the processing capabilities to reduce the requirements of digitized fronthaul in terms of data rates, latency and jitter tolerance, or to increase centralization and transition to a fully analog fronthaul. The latter is enabled through the use of analog radio-over-fiber (ARoF), where the analog waveforms are transported over the ODN, possibly together with an optical local oscillator (LO) to simplify mm-wave upconversion of the signal and minimize complexity at the remote unit (RU) [10]. Combining seamlessly with optical beamforming, ARoF fronthaul with optical beamforming networks (OBFNs) can improve upon network capacity through improved frequency re-use and may reduce the cost and power consumption of the RU by allowing true multi-beam transmission from a single antenna array [11].

While spatial control and multiplexing of the signal are commonly expected in the RF domain, space division multiplexing (SDM) in the optical domain is less well established, especially for the metro- and access segments of optical networks [12]. Nonetheless it offers important potential for ODNs and RANs as it can drastically increase capacity and provides increased flexibility as far as switching, routing and resource assignment are concerned [5, 13]. In time and synchronization critical situations or situations that require the transport of signals in parallel channels, as may be the case for ARoF fronthaul with optical beamforming, the use of multi-core fibers (MCFs) introduces

the availability of multiple independent fiber channels with very similar transmission characteristics.

Combining SDM transport in the ODN with ARoF fronthaul and optical beamforming is the core technology proposition of the EU H2020 5G-PPP project blueSPACE [14]. A successful demonstration of ARoF fronthaul for high-bandwidth mm-wave 5G NR signals using full real-time processing in an ARoF baseband unit (BBU) and multi-core fiber (MCF) transport was demonstrated and discussed in a paper at EuCNC 2020 [15]. This manuscript expands upon this demonstration, discussing the full blueSPACE architecture and providing a detailed description of the concepts and experimental setup, especially the ARoF BBU and real-time digital signal processing (DSP) which are described in detail for the first time. The demonstrated ARoF fronthaul link achieves real-time transmission of 800 MHz wide extended 5G NR orthogonal frequency division multiplexing (OFDM) signals over 10 km of 7-core MCF and 9 m mm-wave wireless at 26.5 GHz, i.e., in the 3GPP FR2 n258 band [6]. The link further used a remote-fed LO for signal downconversion at the RU, avoiding the need for any RF oscillators at the remote site and maximizing centralization of network resources. Together these prove the viability of ARoF fronthaul and demonstrate the core concepts of the blueSPACE fronthaul architecture.

The remainder of this manuscript is structured as follows: Sect. 2 introduces the blueSPACE fronthaul architecture, while Sect. 3 discusses the demonstration setup, providing a detailed description of the real-time DSP in the ARoF BBU (Sect. 3.1) and introducing the experimental setup (Sect. 3.2). Section 4 discusses the performance of the ARoF transmitter (Sect. 4.1) and provides transmission performance measurements for the overall real-time ARoF fronthaul link (Sect. 4.2). Finally, Sect. 5 summarizes and concludes the manuscript.

2 Analog fronthaul with optical beamforming for mm-wave 5G

The centralization of resources in RANs has provided substantial reductions in the cost of network ownership, operation and maintenance, by removing baseband (BB) processing from remote sites and centralizing it in a central office (CO) [16]. This centralization of BB processing resources in a BBU pool at the CO allows C-RAN deployments to use statistical multiplexing and sharing of processing resources to avoid overprovisioning. It further simplifies the management and maintenance of the network by reducing complexity placed at remote locations and at the antenna sites. The downside to this centralization of resources is the introduction of a new RAN segment between the BBU at the CO and the RU at the antenna site, referred to as the fronthaul segment [9, 16].

In current 4G LTE networks where bandwidths and frequencies are limited, this segment is covered by transmitting digitized in-phase and quadrature (IQ) samples of the target radio waveform using traditional BB optical links, detecting the signal at the RU and performing digital-to-analog conversion there (and vice versa for uplink (UL) direction). Such transmission of digitized samples, typically using CPRI and referred to as digitized radio-over-fiber (DRoF), however requires constant bitrate signals, where the latter scales with signal bandwidth and antenna configuration, is independent of user presence or activity, and is highly sensitive to latency and jitter [17]. In more complex deployments using multi-sector antennas, MIMO transmission or larger aggregated

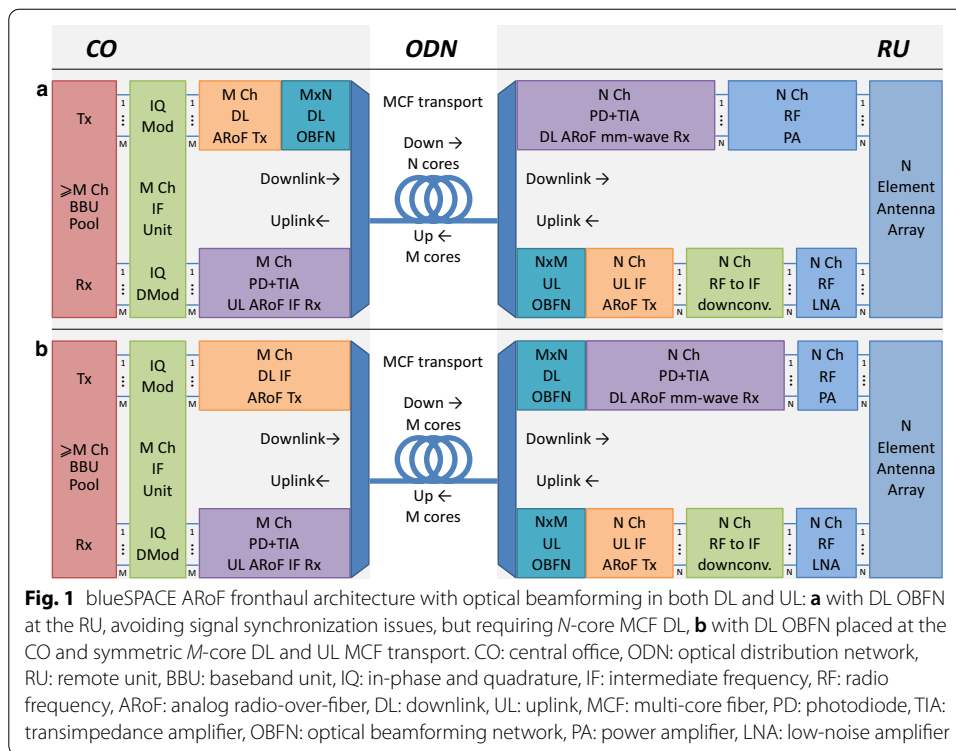Rommel *et al. J Wireless Com Network*   (2021) 2021:43

Page 4 of 20

bandwidths, the data rates required for such fronthaul links quickly scales to hundreds of Gbit/s and into the Tbit/s. As a result, they are clearly not a scaleable solution of high-bandwidth 5G signals, especially at mm-wave where radio bandwidths will be substantially larger than in the sub-6 GHz spectrum.

Two opposite approaches have emerged to address this fronthaul bottleneck for 5G networks, either remaining with DRoF fronthaul, but moving some functionality/processing steps back to the RU or to some intermediate distributed unit (DU), resulting in different functional splits and giving rise to new protocols such as enhanced common public radio interface (eCPRI) or next generation fronthaul interface (NGFI), or increasing centralization and transitioning to analog fronthaul with ARoF [11, 18]. The latter increases centralization by also moving the digital to analog converter (DAC) and analog to digital converter (ADC) from the radio sites to the CO and relies on optical transport of the target RF or intermediate intermediate frequency (IF) waveforms [11, 19]. If the RF waveform is transported or optical heterodyning is used for IF to mm-wave upconversion, ARoF further allows centralizing all RF oscillators and simplifies the mm-wave generation process [20]. ARoF also minimizes the required optical spectrum in the ODN, as the required bandwidth matches the RF bandwidth—although additional bandwidth is needed if optical heterodyning is used, which in turn may be reduced by interleaving channels, e.g., in ultra-dense wavelength division multiplexing (UD-WDM) passive optical networks (PONs) [21, 22].

In addition, ARoF ideally combines with optical beamforming, where analog beamforming is performed in the optical domain, rather than in the RF domain after optical to electrical (O/E) conversion. This brings multiple advantages, including a reduction in spatial, power and cost footprints as well as the possibility to implement full Blass matrices in integrated OBFNs, allowing true multi-beam transmission from a single phased array antenna (PAA) and affording good spatial control over the mm-wave RF signals [23, 24].

In blueSPACE, an ARoF fronthaul architecture with optical beamforming is combined with SDM in the ODN to truly solve the capacity bottleneck in the fronthaul segment. The introduction of MCF as fibre medium for the ODN brings a direct increase in capacity, but also allows another degree of flexibility when it comes to resource allocation or network sharing. The blueSPACE ARoF architecture is shown in Fig. 1, with the ARoF BBU pool and IF unit, the ARoF fronthaul segment with OBFNs for both downlink (DL) and UL as well as the radio equipment with amplifiers and antenna array.

When it comes to the use of optical beamforming in ARoF fronthaul as in the blueSPACE architecture, the placement of the OBFN has significant consequences for the fronthaul transport and may pose specific requirements to the ODN. This is due to the functionality of the OBFN which maps each of its M independent input signals (in DL direction destined for M independent beams) onto each of its N outputs with different differential delays, allowing to independently modify each beam's direction while transmitting all M beams from a single N-element antenna array. As the temporal relation between the N output signals of the OBFN carries the beamforming information, these relations must be precisely preserved from the OBFN to the antenna array element, with the required precision determined by the RF frequency—e.g., in the case of mm-wave transmission around 30 GHz, temporal relation between the beamformed signals

Fig. 1 blueSPACE ARoF fronthaul architecture with optical beamforming in both DL and UL: **a** with DL OBFN at the RU, avoiding signal synchronization issues, but requiring *N*-core MCF DL, **b** with DL OBFN placed at the CO and symmetric *M*-core DL and UL MCF transport. CO: central office, ODN: optical distribution network, RU: remote unit, BBU: baseband unit, IQ: in-phase and quadrature, IF: intermediate frequency, RF: radio frequency, ARoF: analog radio-over-fiber, DL: downlink, UL: uplink, MCF: multi-core fiber, PD: photodiode, TIA: transimpedance amplifier, OBFN: optical beamforming network, PA: power amplifier, LNA: low-noise amplifier

must be maintained within $\approx 1\,\mathrm{ps}$ to avoid significant deformation of the beams [25]. In UL direction, the same is true and temporal alignment must be maintained from the antenna array to the N inputs of the OBFN, which de-maps the received signals and spatially filters them to output the signal from M different received beams on its M outputs.

Figure 1a shows the first option, with the OBFNs for DL and UL located with the corresponding ARoF transmitters, i.e., the DL OBFN at the CO and the UL OBFN at the RU. While this configuration allows centralization of the DL OBFN and thus maintains a simpler RU, it does require signals to remain temporally aligned across transport in the ODN. The latter is a major challenge and would be impossible to achieve using separate single-mode fiber (SMF), fibre bundles or single-mode fiber (SMF) ribbon cables and even with the use of MCF, which does provide better temporal alignment, may be problematic [26]. For the DL direction, the same would apply if the OBFN were to be centralized, however with placement at the RU, as shown in Fig. 1, this issue does not arise as the entire critical path—from the antenna array, across the downconversion stage and until the output of the OBFN—is located at the RU. Furthermore, in this scheme the number of channels that are transported across the ODN for DL and UL is asymmetric, with the number of DL channels scaling with the number of antenna elements N and the number of UL channels scaling with the number of beams M. As typically $N > M$, often substantially so, this poses questions to network occupation and may ultimately limit the size the antenna array can be scaled to, as it may not be possible to equally scale the number of cores in the MCF.

To avoid the necessity to maintain temporal alignment across the ODN, the DL OBFN may be placed at the RU, as shown in Fig. 1, which results in a symmetric number of

channels for DL and UL, both scaling with the number of beams M. There is thus a clear trade-off between complexity at the RU through having the OBFN there and requirements on the ODN. It should further be noted that, if the OBFN is based on optical phase shifting and optical heterodyning is used for mm-wave upconversion, temporal relation may need to be maintained starting at the ARoF transmitter, unless both signal and second tone are transported in the same fiber. Thus, the scheme in Fig. 1b may need to be upgraded, e.g., though the introduction of an additional O/E/O step between MCF and OBFN to guarantee signal alignment while also potentially improving link power budget, but at the cost of increased complexity, cost and power consumption at the RU.

3 High-capacity ARoF fronthaul demonstration experimental setup

To demonstrate the core concepts of the proposed ARoF fronthaul architecture, an experimental setup is established, including the ARoF BBU with real-time DSP, ARoF signal generation and optical heterodyning for mm-wave generation and the ODN with MCF for signal transmission. While optical beamforming is an integral part of the proposed architecture and improves the mm-wave link power budget through concentration of the radiated energy in a smaller area, as well as greatly enhancing system spectral efficiency (SE) by allowing denser frequency reuse, it is not included in this demonstration, as a simple point-to-point ARoF link must be shown and evaluated first. The following will first detail the architecture, signal processing chain and supported functionality of the ARoF BBU (Sect. 3.1), before discussing the overall fronthaul demonstration setup in detail (Sect. 3.2).

3.1 5G NR signal generation and real-time processing

The blueSPACE ARoF BBU core, implemented in a field programmable gate array (FPGA) device [27], provides all the DSP required to generate and handle the 5G NR OFDM signals to be transmitted. The OFDM waveform is represented in BB by two components, the in-phase (I) and quadrature (Q) components, each with half the bandwidth of the desired radio waveform. The BB signals are converted from the digital to the analog domain and vice versa by multi-channel DACs and ADCs [28, 29]. The blueS-PACE BBU mainly consists of five modules, i) the digital data interface acting as data source/sink for the DSP chains, ii) the cyclic prefix (CP) OFDM transmitter side DSP datapath, iii) the CP-OFDM receiver side DSP datapath, iv) the analog data interface towards DAC and ADC, and v) the embedded central processing unit (CPU). The interconnection of these modules and their internal structure are shown in Fig. 2.

3.1.1 Digital interface—data source/sink

This bidirectional digital interface acts as a source of data for the transmitting side of the BBU (DL) and as a sink for the receiving side (UL). A 10 Gbit/s ethernet interface is provided for interconnection with the backhaul, while an embedded bit error rate tester (BERT) can be used for debugging and evaluation of the link performance. The BERT employs 32-bit interfaces, both for the transmitter and receiver sides and it is clocked at 245.76 MHz, reaching a peak data rate of 7864.32 Mbit/s in each direction, which is sufficient to support the peak data rate supported by the BBU. The 10 Gbit/s ethernet interface is implemented using the low latency ethernet 10G medium access control (MAC)
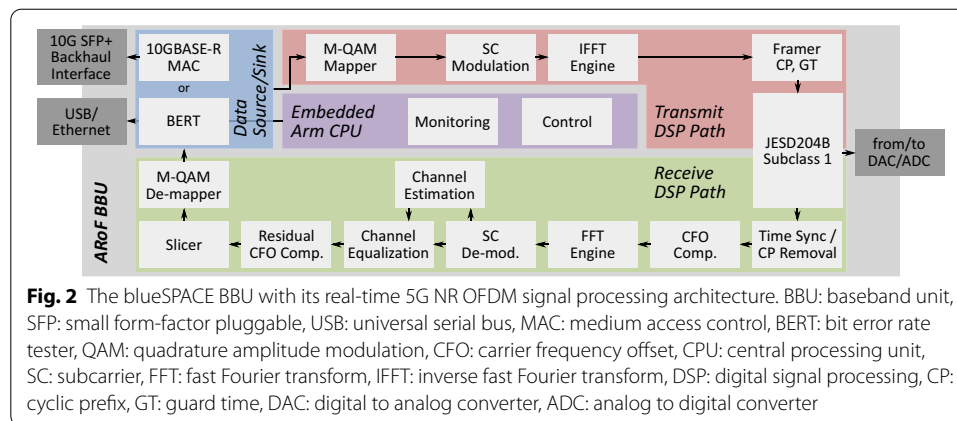
Fig. 2 The blueSPACE BBU with its real-time 5G NR OFDM signal processing architecture. BBU: baseband unit, SFP: small form-factor pluggable, USB: universal serial bus, MAC: medium access control, BERT: bit error rate tester, QAM: quadrature amplitude modulation, CFO: carrier frequency offset, CPU: central processing unit, SC: subcarrier, FFT: fast Fourier transform, IFFT: inverse fast Fourier transform, DSP: digital signal processing, CP: cyclic prefix, GT: guard time, DAC: digital to analog converter, ADC: analog to digital converter

Intel FPGA IP core [30]. The physical interface for this interface is a small form-factor pluggable (SFP)+ module (10GBASE-R), while the interface with the BBU is a bidirectional 64-bit interface clocked at 156.25 MHz, providing a peak data rate of 10 Gbit/s in each direction. Rate matching between this interface and the BBU digital interface is provided using a pair of dual-clock first-in, first-out (FIFO) memories.

3.1.2 Transmit DSP datapath

The transmitter DSP performs 5G NR OFDM signal generation and supports a number of transmission modes [6, 31], as shown in Table 1. This module receives plain digital data, originating from either of the sources in the digital interface, and exports data samples that describe the analog BB signals towards the analog interface which drives the DACs. The incoming bits are grouped into symbols, according to the selected constellation size, using Gray coding. Supported constellations are quadrature phase-shift keying (QPSK) and quadrature amplitude modulation (QAM) (16-QAM, 64-QAM and 256-QAM) [31]. The constellation can be selected through a dedicated register in the register file, which can be updated on the fly through software. From this point on, all data is represented as complex numbers.

The resulting symbols are used to modulate the available OFDM subcarriers. The number of available subcarriers and their position in the spectrum can be programmed on the fly using a dedicated random access memory (RAM), which can be written through software. This module also provides the flexibility to set the number and position of the pilot subcarriers used for channel estimation at the receiver side. Pseudo random bit sequences (PRBSs) based on length-31 Gold sequences are used for pilot subcarriers, providing better cross-correlation properties than maximum length linear-feedback shift register (LFSR) sequences, as defined in [31]. All subcarriers, either carrying data or pilot symbols can be set in blocks of four, as four subcarriers are always processed in parallel during each clock period with a clock frequency of 245.76 MHz, which is equal to $\frac{1}{4}$ of the maximum sampling rate of 983.04 MSa/s. The maximum number of modulated subcarriers is 3168 and corresponds to 264 resource blocks (RBs), as defined by 3GPP [6]. Modulated subcarriers (in the frequency domain) are transformed to the time-domain using a 4096-point inverse fast Fourier transform (IFFT) engine.

Rommel *et al. J Wireless Com Network* (2021) 2021:43

Page 8 of 20

Table 1 Transmission modes supported by the blueSPACE ARoF BBU and corresponding signal and DSP parameters

Mode	Numerology (μ)	Subcarrier spacing [kHz]	FFT size	Sampling frequency [MHz]	Slots/sub-frame	Slot duration [µs]	Max. num of active subcarriers	Max. bandwidth [MHz]	Theoretical max. Bitrate [Mbit/s]	Modulation formats
M2	2	60	4096	245.76	4	250	3168	190.08	1419.3	QPSK, 16QAM, 64QAM, 256QAM
M2E	2	60	4096	245.76	4	250	3168	190.08	1216.5	
M3	3	120	4096	491.52	8	125	3168	380.16	2838.5	
M4	4	240	2048	491.52	16	62.5	1584	380.16	2838.5	
M4bS*	4	240	4096	983.04	16	62.5	3168	760.32	5677.1	

* Extended version of mode M4 introduced by blueSPACE through extrapolation of the 5G NR numerology to maximize transmission capacity and show up to 800 MHz RF bandwidth

This engine instantiates four 1024-point IFFT engines operating in parallel and combines their outputs using a radix-4 decimation in time (DIT) butterfly unit. The Intel fast Fourier transform (FFT) IP core [32] is used for the 1024-point FFT engines.

The framer module introduces the CP and guard time (GT) required to form a complete OFDM symbol. CP and GT are set using dedicated registers in the register file which can be updated on the fly by software. The final transmitter DSP stage includes all processing performed in the time domain and provides a total of 30 dB of digital gain, adjustable in steps of 6 dB, before signals are output towards the analog interface.

3.1.3 Receive DSP datapath

The receiver DSP performs 5G NR OFDM signal demodulation and supports the same transmission modes supported by the transmitter DSP, as shown in Table 1. This module receives data samples of the incoming analog signals, as encoded by the ADCs, from the analog interface and exports the decoded digital data to the digital interface, destined for either the backhaul interface or the built-in BERT for bit error rate (BER) measurements. Rate matching with the external digital interface is again provided using a dual clock FIFO memory.

From the incoming data, the in-phase signal is mapped to the real part of the complex numbers used for further processing, while the quadrature signal is mapped to the imaginary part. The first receiver DSP stage includes all processing performed in the time domain and provides a total of -30 dB of digital gain, adjustable in steps of -6 dB. This stage compensates for the digital gain set at the transmitter side, while the combination of these two stages is used to optimize the signal-to-noise ratio (SNR) of the received signal by adjusting to link power budget conditions.

The incoming signal is synchronized using autocorrelation techniques, where the incoming signals are compared with delayed versions of the same signal. This delay can be adjusted and in normal operation is equal to the length of the FFT. After synchronization, the CP is removed from the received data. The carrier frequency offset (CFO) is estimated using a maximum likelihood (ML) technique [33], while the estimated value controls a numerically-controlled oscillator (NCO), which allows the frequency to be set with a resolution of 0.05722 Hz. The CFO is then compensated by simple multiplication of the synchronized data with the output of the NCO. The CFO estimation can be entirely bypassed or combined with a value set at the proper registers in the register file for debugging purposes.

The FFT engine is similar to the IFFT engine in the transmitter DSP, also combining the outputs of four 1024-point FFT engines using a radix-4 DIT butterfly unit to transform an incoming OFDM symbol from the time domain (samples) to the frequency domain (subcarriers). All modulated subcarriers are extracted in the reverse fashion as the subcarrier modulation in the transmitter DSP, while subcarriers not carrying data or pilot information are discarded. Subcarriers carrying payload are directed to the channel equalization unit, while pilot subcarriers are forwarded to the channel estimation unit. The channel estimator compares the received pilot subcarriers with the transmitted pilot subcarriers and feeds a zero-forcing equalizer. The channel estimator, similar to the transmitter side, is equipped with a length-31 Gold sequence generator to generate the pilot symbols on the fly, according to the modulation scheme information that is written

to its dedicated RAM. Although the NCO frequency resolution is $\approx 0.05\,$Hz, this is not small enough for the receiver to acquire and process data for several seconds without re-training the equalizer. The remaining carrier frequency offset is expressed as a tilt in the constellation that slowly rotates, making BER calculation impossible. The residual CFO compensation module continuously estimates the rotation angle and compensates it using vector rotators.

Finally, the symbol estimation/slicer estimates the received symbols by calculating the Euclidean distances between the received symbol and the used constellation and selecting the symbol with the minimum distance. The detected QAM or QPSK symbols are then de-mapped into plain bits using Gray decoding.

3.1.4 Analog interface

This is a digital high bit rate serial interface between the FPGA and the DACs and ADCs. Although still digitally carrying digital signals, this is the FPGA design analog interface as it coordinates the translation to/from the analog domain. The Intel JESD204B FPGA IP [34] has been used for the implementation of this interface. The DAC and ADC interfaces each use a single link JESD204B subclass 1 interface that employs four lanes operating at 9.8304 Gbit/s, reaching a total throughput of 39.3216 Gbit/s including 8b/10b encoding. The employed DAC resolution is 16 bit, while the actual ADC resolution is 12 bit, but 16 bit are sent per sample to ease future upgrades.

3.1.5 Embedded CPU

The CPU embedded with the FPGA allows for control and monitoring of the BBU via a ethernet and universal serial bus (USB) interfaces. The embedded CPU is a dual-core ARM Cortex-A9 hard processor system [35] running at 1.2 GHz that is implemented on the same chip with the Arria 10 FPGA device and has access to 1 GB of DDR4-2133 RAM. Communication between the FPGA and the CPU is realized with multiple advanced eXtensible interfaces (AXIs). The operating system running on the embedded CPU is Angstrom Linux.

3.2 Analog radio-over-fiber transmission setup

The ARoF fronthaul demonstration for high-capacity mm-wave 5G signals implements the core components of the blueSPACE ARoF architecture shown in Fig. 1, ARoF signal generation, MCF fronthaul transport and optical heterodyning for mm-wave signal generation—the corresponding reduced architecture is shown in Fig. 3. Beyond the blueS-PACE ARoF BBU unit described in the previous section, this contains the IF unit and ARoF transmitter at the CO, the shared MCF for transport of DL and UL ARoF signals as well as the remote-fed LO, the RU for O/E conversion and RF signal radiation to the UE. The ARoF transmitter includes an RF LO for two-tone generation, while at the RU both the mm-wave RF DL signal and the RF LO used for downconversion of the UL signal are generated through optical heterodyning, avoiding the need for an RF oscillator in the remote location.

The experimental setup employed in this demonstration implements this core ARoF architecture based on commercially available optical and RF components at the CO and RU, while the MCF and corresponding fan-in and -out modules were specifically
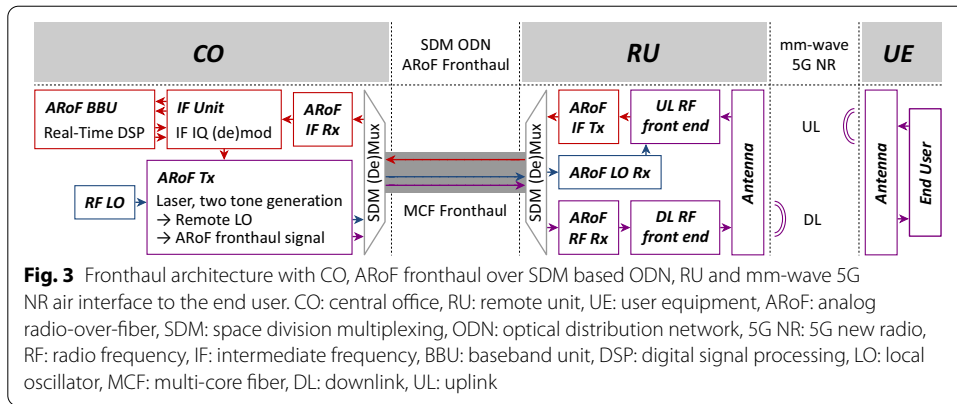
Fig. 3 Fronthaul architecture with CO, ARoF fronthaul over SDM based ODN, RU and mm-wave 5G NR air interface to the end user. CO: central office, RU: remote unit, UE: user equipment, ARoF: analog radio-over-fiber, SDM: space division multiplexing, ODN: optical distribution network, 5G NR: 5G new radio, RF: radio frequency, IF: intermediate frequency, BBU: baseband unit, DSP: digital signal processing, LO: local oscillator, MCF: multi-core fiber, DL: downlink, UL: uplink
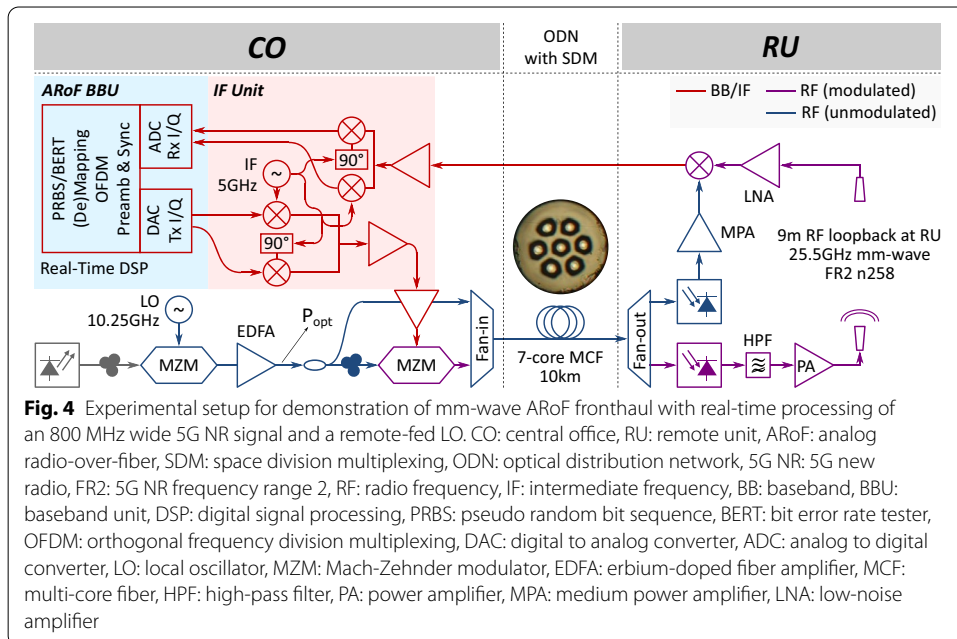

Fig. 4 Experimental setup for demonstration of mm-wave ARoF fronthaul with real-time processing of an 800 MHz wide 5G NR signal and a remote-fed LO. CO: central office, RU: remote unit, ARoF: analog radio-over-fiber, SDM: space division multiplexing, ODN: optical distribution network, 5G NR: 5G new radio, FR2: 5G NR frequency range 2, RF: radio frequency, IF: intermediate frequency, BB: baseband, BBU: baseband unit, DSP: digital signal processing, PRBS: pseudo random bit sequence, BERT: bit error rate tester, OFDM: orthogonal frequency division multiplexing, DAC: digital to analog converter, ADC: analog to digital converter, LO: local oscillator, MZM: Mach-Zehnder modulator, EDFA: erbium-doped fiber amplifier, MCF: multi-core fiber, HPF: high-pass filter, PA: power amplifier, MPA: medium power amplifier, LNA: low-noise amplifier

designed and fabricated for and in the blueSPACE project. The MCF is a 7-core MCF with a central core and six outer cores positioned in a circle around the central core, as seen in the inset of Fig. 4. The MCF is designed to emulate the transmission properties of standard SMF, achieving similar chromatic dispersion ($\approx 19\,\mathrm{ps/nm/km}$) and loss ($\approx 0.25\,\mathrm{dB/km}$), with an overall insertion loss of $\approx 4.5\,\mathrm{dB}$ for 10 km MCF including the fan-in and -out modules from/to separate SMFs.

A detailed schematic of the experimental setup is shown in Fig. 4. The IF unit is the link between the signal processing in the BBU and the ARoF fronthaul link. It upconverts the DL analog BB IQ signals from the DAC in the BBU to an IF f_{IF} in the range of 2.25 GHz to 5.5 GHz based on a tunable locally generated LO, which is also used for downconversion of the received UL IF signal into separate BB IQ signals that can be input to the ADC of the BBU. The IF unit further contains amplifiers to boost the generated DL IF signal as well as to pre-amplify the received UL IF signal before

demodulation; a pair of low-pass filters (LPFs) (not shown in Fig. 4) is used to filter the signal to remove undesired higher frequency components from the generated and received IF signals.

The ARoF transmitter is based on an external cavity laser (ECL) with a linewidth of ≈ 25 kHz and performs two-tone generation with a Mach-Zehnder modulator (MZM) biased at the null point for carrier suppression and driven with an LO at f_{LO}. The generated two-tone signal is amplified to an output power P_{opt} of 18 dBm by an erbium-doped fiber amplifier (EDFA) and split equally into two parts—one is directly transmitted over the MCF to the RU to be used as remote-fed LO, while the other is modulated with the amplified data-carrying IF signal from the IF unit in a second MZM. The latter is biased at the quadrature point to ensure linear transmission of the IF signal. It should be noted, that the selected frequency doubling scheme with suppression of the original carrier eliminates the problem of dispersion induced carrier fading [36], while the use of an IF avoids the issue of signal-signal beat noise [37].

The generated ARoF and LO signals are transmitted to the RU through separate cores of the MCF and through optical heterodyning on a high-speed photodiode (PD) generate the desired modulated DL mm-wave RF signal at $f_{RF} = 2f_{LO} + f_{IF}$ as well as the mm-wave LO at $2f_{LO}$ used for dowconversion of the received UL mm-wave RF signal. Undesired lower frequency components of the mm-wave RF signal are removed by a high-pass filter (HPF), before amplification by 30 dB using a power amplifier (PA).

Wireless transmission at 25.5 GHz over 9 m distance is performed using a pair of pyramidal horn antennas with a gain of 18.5 dBi gain each, forming a loopback at the RU. The latter both simplifies the experimental setup and realistically emulates a DL transmission link, containing a single optical and mm-wave wireless transmission respectively, as would be experienced by DL transmission to a UE. The received signal at the RU, which in a real scenario would be the received signal from the UE, is amplified by 40 dB using a low-noise amplifier (LNA) and downconverted to IF using the remote-fed LO, which results from the heterodyning of the pure two-tone signal transmitted from the CO with an additional amplification by 30 dB in a medium power amplifier (MPA) to achieve sufficient LO levels to drive the mixer. While, as shown in Fig. 3, in a real scenario the downconverted IF signal would be transported back to the CO over a separate core of the MCF, in the experimental setup it is fed directly to the receiving UL side of the IF unit, effectively using it as UE and maintaining a realistic emulation of a DL transmission.

It should be noted that through the proposed implementation of the ARoF fronthaul architecture shown in Fig. 3 a substantial reduction of complexity of the RU is achieved. First, optical heterodyning for mm-wave generation and the remote-fed LO for downconversion allow centralization of all RF oscillators at the CO, leaving only RF amplifiers and the mixer. Second, optical intermediate frequency-over-fiber (IFoF) transmission of the UL signal will require modulation of an optical signal with the received IF—the required optical carrier can easily be provided from the CO across the MCF, either at a different wavelength sharing a core with the LO or ARoF signals or over a separate core, leaving only the modulator at the RU. Similarly, the proposed

setup and architecture avoids the use of any optical amplifiers in the ODN or at the RU, requiring optical amplification only in two-tone generation.

4 Real-time analog fronthaul demonstration results and discussion

The evaluation of the proposed ARoF setup and its associated transmission performance involves, first, the analysis of the transmission setup, showing associated optical and electrical spectra (Sect. 4.1), and, second evaluation of transmission performance based on BER and error vector magnitude (EVM)/received constellations after real-time signal processing in the ARoF BBU (Sect. 4.2).

4.1 Analog radio-over-fiber transmission

The optical two-tone generation and ARoF transmitter setup has a fundamental impact on the performance of the overall link, as it defines the targeted RF frequency and largely determines the levels of phase noise in the final RF signal generated through the optical heterodyning. In this demonstration, the targeted RF frequency is towards the lower end of the 3GPP FR2 n258 band, which ranges from 24.25 GHz to 27.5 GHz, and is set to be $f_{RF} = 25.5$ GHz, composed of the two-tone signal spacing plus the IF frequency, as:

$$\begin{aligned} f_{RF} &= 2f_{LO} + f_{IF} \\ &= 2 \cdot 10.25\,\text{GHz} + 5\,\text{GHz} = 25.5\,\text{GHz}, \end{aligned} \tag{1}$$

as can be seen in Fig. 5.

First, for the generation of the two-tone signal, it is important to suppress all unnecessary signal components in order to minimize resulting undesired beating products during the optical heterodyning for mm-wave RF signal generation. Careful optimization of bias voltage and driving amplitude allows to achieve ≈ 30 dB of suppression between the desired tones spaced at $2f_{LO}$ and the original carrier as well as higher order odd and even harmonics respectively, as seen for the two-tone LO output in Fig. 5. Second, modulation with the IF signal should be performed with driving power and bias point optimized
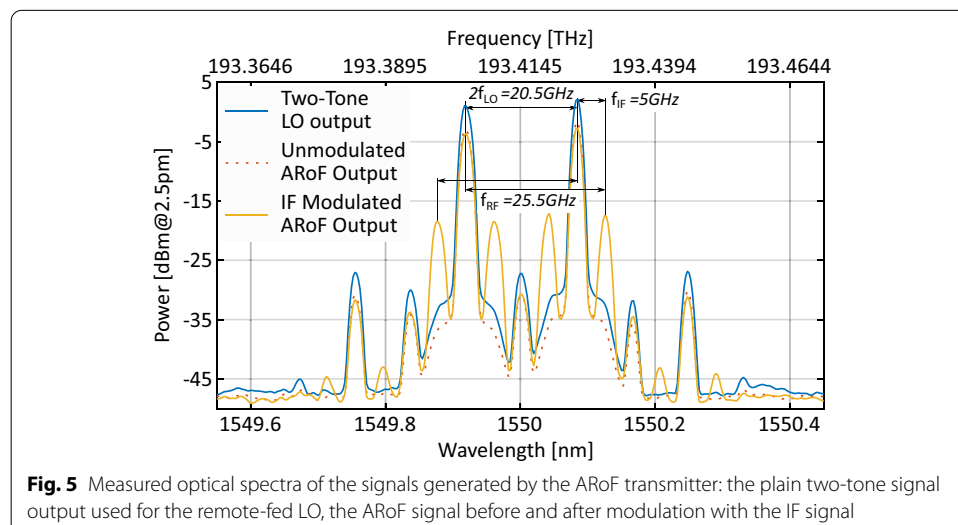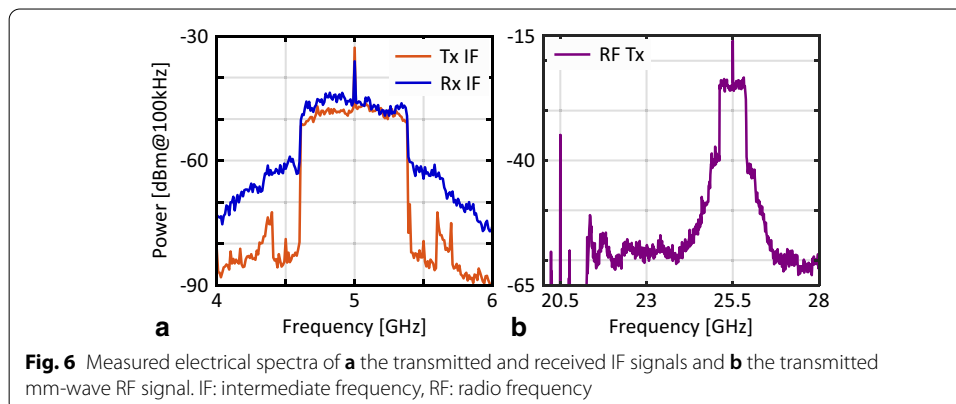

Fig. 5 Measured optical spectra of the signals generated by the ARoF transmitter: the plain two-tone signal output used for the remote-fed LO, the ARoF signal before and after modulation with the IF signal

so that the full linear range of the MZM transfer function is used, while avoiding the compression regions to prevent distortion of the carried OFDM signal. The resulting ARoF output signal after the second MZM is also shown in Fig. 5, both in unmodulated and modulated form. The latter clearly shows the IF signal modulated on top of both tones of the two-tone signal, resulting in a pair of tones spaced at f_{IF} around each.

The IF signal, as generated by the IF unit, i.e., before amplification for driving the MZM is shown in Fig. 6a, showing it centered at $f_{IF} = 5\,\text{GHz}$ as required to achieve the targeted RF frequency according to Eq. 1. It should be noted that the 800 MHz wide OFDM data signal is clearly visible and a carrier-to-signal ratio (CSR) of $\approx 15\,\text{dB}$ is observed, while the SNR is $\approx 35\,\text{dB}$.

Given the optical ARoF signal shown in Fig. 5, it is clear that the beating on the PD will generate the desired modulated RF signal at $f_{RF} = 2f_{LO} + f_{IF}$, but will also generate signals at other multiples of f_{LO} and its combinations with f_{IF}. The majority of these are removed through the HPF after the PD, while higher frequency products are mostly outside the bandwidth of the PA used before the radiating antenna. The resulting RF signal after amplification is shown in Fig. 6b, where it should be noted that the tone at 20.5 GHz, i.e., the direct beating of the two-tone signal, is insufficiently suppressed with an approximately equal tone at 30.75 GHz not shown—in a system destined for deployment these could easily be suppressed by replacing the HPF with a band-pass filter (BPF) and limiting PA bandwidth to the required band in order to adhere to out-of-band and spurious emission limits set by relevant standardization [6].

The received IF signal after mm-wave transmission, amplification in the LNA and downconversion using the remote-fed LO is shown in Fig. 6a, showing a similar power level as the transmitter IF signal, but with SNR reduced to $\approx 12\,\text{dB}$. The received IF signals further shows a somewhat reduced CSR which, together with the shape of the noise around the signal, suggests the presence of nonlinearities in the link, likely due to saturation of either the PA or LNA. Finally, the received IF signal appears slightly tilted, with powers of the higher frequency subcarriers somewhat lower than for the lower frequency subcarriers. The latter is likely caused by the LPF used at the input to the IF unit, as it has a 3 dB cut-off frequency of 5.5 GHz and will thus cause some attenuation already at frequencies between 5.0 and 5.5 GHz.

Fig. 6 Measured electrical spectra of **a** the transmitted and received IF signals and **b** the transmitted mm-wave RF signal. IF: intermediate frequency, RF: radio frequency
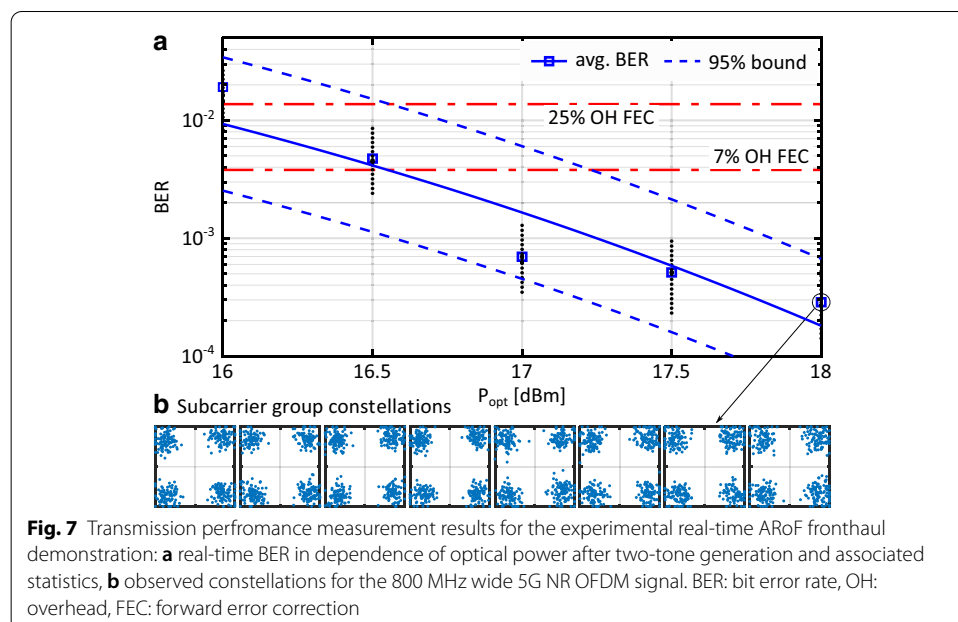
4.2 Real-time transmission performance

To evaluate transmission performance, EVM and BER are measured after real-time processing at the BBU for a range of optical powers P_{opt} after two-tone generation. As varying optical power varies both RF and LO power after heterodyning, even small changes in optical power cause substantial changes in the final received IF power: from the square-law detection principle of the PD and as varying P_{opt} varies the power in both tones, a 1 dB change in optical power directly corresponds to a 2 dB change in both RF and LO powers. Furthermore, due to reduced downconversion efficiency in the mixer at the RU for lower LO powers, an additional 1 dB of degradation is estimated for every 2 dB reduction in LO power—causing an overall reduction of 5 dB in received IF power for every 1 dB of optical power reduction.

The BER of the received signal is evaluated continuously by the ARoF BBU and retrieved repeatedly after short time intervals for each measured optical power. The separate measured BER values are shown in Fig. 7a, which also shows their average and corresponding 95% confidence bounds for the BER in any such short time interval, derived from the measured BER statistics. This suggests significant variation of BER over time does occur and that a sufficient margin must correspondingly be considered for any real system implementation.

It also proves successful transmission of a 5G NR OFDM signal using the extended M4bS mode shown in Table 1, showcasing seamless transmission with an RF bandwidth of 800 MHz at 25.5 GHz and thus in the 3GPP FR2 n258 mm-wave band. The system demonstrates transmission at a data-rate of 1.4 Gbit/s after 10 km MCF and 9 m mm-wave wireless using fully real-time processing in the ARoF BBU for both signal generation and analysis.

Figure 7a further indicates the BER limits of 3.8×10^{-3} and 1.3×10^{2} for typical forward error corrections (FECs) with 7% and 25% overhead (OH), respectively. This shows

Fig. 7 Transmission perfromance measurement results for the experimental real-time ARoF fronthaul demonstration: **a** real-time BER in dependence of optical power after two-tone generation and associated statistics, **b** observed constellations for the 800 MHz wide 5G NR OFDM signal. BER: bit error rate, OH: overhead, FEC: forward error correction

Rommel *et al. J Wireless Com Network*   (2021) 2021:43

Page 16 of 20

the system easily achieves these limits depending on transmitted power and suggests that with further optimization and the substantially more complex FEC codes routinely used in mobile communications higher order constellations could be achieved—substantially increasing both data rates and SE.

Finally, Fig. 7b shows the observed constellations of the received signal after downconversion to BB, digitization and OFDM processing, with eight subcarrier groups, each corresponding to ≈ 100 MHz of RF spectrum, shown as separate constellations for easier comparison. It should be noticed that although they are shown in separate constellations, all subcarriers are jointly processed during the real-time DSP. The observed constellations match the expectations for the estimated EVM of $\approx 20\%$. While the latter is above the limit for FR2 base station emission as defined by 3GPP [6] of 17.5% to 19%, it should be noted that the latter is set for transmission from the RU, while that measured here includes wireless transmission and the associated EVM degradation, suggesting the signal radiated from the RU to be within the specified limits.

5 Conclusions

This article presented the blueSPACE fronthaul architecture with ARoF transport over SDM and optical beamforming and showed a demonstration of a high-bandwidth mm-wave 5G NR signal transmission with ARoF fronthaul over MCF. The blueSPACE architecture introduces the combination of ARoF with SDM in the ODN to solve the fronthaul capacity bottleneck and uses optical beamforming to seamlessly enable multibeam transmission and achieve spatial control over the RF signal.

The demonstrated fronthaul link used the blueSPACE ARoF BBU for real-time signal processing of 800 MHz extended 5G NR OFDM signals, which are upconverted to a tunable IF between 2.25 GHz and 5.5 GHz. Combined with the fixed LO of the ARoF transmitter this allows the demonstrated link to cover the entire 3GPP FR2 n258 band between 24.25 GHz and 27.5 GHz. The real-time fronthaul link achieves data rates of 1.4 Gbit/s with BERs below the limit for a 7% OH FEC after transmission over 10 km 7-core MCF and 9 m mm-wave wireless at 25.5 GHz. The demonstrated ARoF fronthaul link further employs a remote-fed LO for electrical downconversion, thus achieving not only minimum optical bandwidth requirements, but also maximum centralization of network functionality and complexity.

The demonstrated real-time fronthaul link highlights the functionality of the blueSPACE ARoF BBU and validates the ARoF fronthaul concept at the heart of the blueSPACE architecture. It further shows a possible use and advantage of SDM using MCF in the RAN. This demonstration proves the feasibility and highlights the potential for timely deployment of such mm-wave ARoF links for high-capacity 5G networks.

Abbreviations
SFP: Small form-factor pluggable; USB: Universal serial bus; 4G: Fourth generation mobile network; 5G: Fifth generation mobile network; ADC: Analog to digital converter; ARoF: Analog radio-over-fiber; BB: Baseband; BBU: Baseband unit; BER: Bit error rate; BERT: Bit error rate tester; BPF: Band-pass filter; C-RAN: Centralized radio access network; CFO: Carrier frequency offset; CO: Central office; CP: Cyclic prefix; CPRI: Common public radio interface; CPU: Central processing unit; CSR: Carrier-to-signal ratio; DAC: Digital to analog converter; DIT: Decimation in time; DL: Downlink; DRoF: Digitized radio-over-fiber; DSP: Digital signal processing; DU: Distributed unit; ECL: External cavity laser; eCPRI: Enhanced common public radio interface; EDFA: Erbium-doped fiber amplifier; EVM: Error vector magnitude; FEC: Forward error correction; FFT: Fast Fourier transform; FIFO: First-in, first-out; FPGA: Field programmable gate array; FR2: Frequency range 2; GT: Guard time; HPF: High-pass filter; I: In-phase; IF: Intermediate frequency; IFFT: Inverse fast Fourier transform; IFoF:

Acknowledgements

Authors' contributions

SR designed the experiment and coordinated its execution to which EG, BC, DD, AM, EP, JB, and GF contributed. EG and EP designed and implemented the BBU and associated DSP. MK, KN, and DK designed and implemented the IF unit and provided guidance with regards to preserving IF and RF signal fidelity. IS, PM, and MD designed, fabricated and provided the MCF fan-in and fan-out modules and provided guidance with regards to signal transmission in the MCF. SR, BC, EP, DD and AM recorded the measurement data, SR performed data analysis and calculated BER statistics. SR, EG and JBC wrote the manuscript. SR, EG, DD, JBC, KN and ITM revised and corrected the manuscript. All authors read and approved the final manuscript.

Authors' information

Simon Rommel obtained his B.Sc. degree from the University of Stuttgart, Germany in 2011 and in 2014 obtained M.Sc. degrees in Photonic Networks Engineering from Aston University, Birmingham, UK and Scuola Superiore Sant'Anna, Pisa, Italy. He completed his Ph.D. in 2017 at the Technical University of Denmark, Kongens Lyngby, Denmark with research focused on photonic-wireless convergence and millimeter-wave radio-over-fiber links. In the same year he visited the National Institute of Information and Communications Technology, Koganei, Tokyo, Japan for a research stay. Since 2017 he is with Eindhoven University of Technology, currently as an assistant professor, continuing his work on photonic and radio frequency technologies with a strong focus on implementations for 5G. His research interests include the fields of fiber-optic and wireless communications and the associated digital signal processing. He has contributed to multiple national and European research projects, incl. H2020 blueSPACE as technical manager. Dr. Rommel is a member of Institute of Electrical and Electronics Engineers (IEEE), The Optical Society (OSA), the Institution of Engineering and Technology (IET) and the Verband der Elektrotechnik Elektronik Informationstechnik e.V (VDE).

Delphin Dodane received the M.Eng. degree in Microelectronics from Grenoble INP Phelma (Grenoble, France) in 2016 as well as the M.Sc. degree in Lasers and Light-Matter Interactions from Université Paris-Saclay (Paris, France) in 2017. He is currently pursuing the Ph.D. degree at Thales Research & Technology (France) and working on Photonic Integrated Circuits for Microwave Photonics applications. He is also involved in the EU H2020 blueSPACE project. His research interests are photonic integrated circuits, semiconductor lasers, microwave photonics and photonic crystals.

Alvaro Morales received the B.Sc. degree in telecommunication technologies engineering and the M.Sc. degree in telecommunications engineering from the University of Valladolid (UVa), Spain, in 2014 and 2016, respectively. He worked as a student assistant at the Photonics Engineering Department, Technical University of Denmark (DTU) between 2015 and 2017. He is currently pursuing the Ph.D. degree at the Technical University of Eindhoven (TU/e), Netherlands, under the framework of the EU H2020 project CELTA. His research interests include millimeter-wave and sub-terahertz communications, radio-over-fiber systems, beamforming and photonic integration.

Evangelos Pikasis received the B.S. degree in Electronics from department of Electronics, in Technological Educational Institute of Athens, the M.Sc. degree in Electronics and Signal Processing and the Ph.D. degree from the National and Kapodistrian University of Athens, in 2005, 2007, and 2014, respectively. From 2008 to 2015 he served as a researcher at the Optical Communications Laboratory, National and Kapodistrian University of Athens, participating in local and European projects. From March 2016 to March 2017, he worked as Postdoctoral Researcher, at School of Engineering of University of Edinburgh. Since June 2017 to July 2020, he worked as DSP and Telecom Engineer at EULAMBIA Advanced Technologies L.t.d. Since September of 2020 he is with Intracom Telecom S.A. as Wireless Research Engineer. His area of expertise includes advanced modulation schemes, Analog Radio over Fiber, Microwave photonics, Digital Signal Processing for RF and Optical communications, DSPs/FPGAs, RF and cryptography at the physical layer.

Juliana Barros Carvalho graduated in Physics with emphasis on Physics Teaching from Federal Rural University of Rio de Janeiro, Brazil. From 2010 to 2016, she worked as researcher at Telecommunications Studies Centre of Pontifical Catholic University of Rio de Janeiro, Brazil, where she obtained her master's and doctoral degree in Electrical Engineering in Applied Electromagnetism. She realized her Ph.D. in the Optical Sensors Laboratory of the Department of Mechanical / Environmental Engineering developing optical fiber sensors for gas monitoring. From 2016 to 2017 she worked in the Brazilian Army Technological Centre as researcher in the development of high frequency circuits for the Saber M200 Radar. In 2018, she was visiting professor at the University of Campinas, Sao Paulo, Brazil, with extensive research on silica optical fibers for use in the infrared sensors, as well as with polymer fibers for THz applications and exploring different applications of additive manufacturing. In the same year, she was at Telecommunications Institute of Aveiro University, Portugal, as a post-doctoral researcher in 5G signal processing applied to an OFDM radar. In 2019 she started a

post-doctoral position at the Terahertz Photonic Systems group of Eindhoven University of Technology, mainly involved in the blueSPACE and BRAINE research projects.

Konstantinos Ntontin received the Diploma in Electrical and Computer Engineering in 2006, the M. Sc. Degree in Wireless Systems in 2009, and the Ph. D. degree in 2015 from the University of Patras, Greece, the Royal Institute of Technology (KTH), Sweden, and the Technical University of Catalonia (UPC), Spain, respectively. His research interests are related to the Physical Layer of wireless telecommunications and particularly to topics such as performance analysis in fading channels, MIMO systems, array beamforming, and stochastic modeling of wireless channels.

Dimitrios S. Kritharidis received his Diploma in Electrical Engineering from National Technical University of Athens, Greece in 1988 and his MSc in Microprocessor Engineering and Digital Electronics from UMIST, U.K. in 1989. After spending a year in Siemens Medical Division, in 1991 he joined INTRACOM, Athens, Greece, as an ASIC Designer. From 1993-2009 he led the IC Design activity in INTRACOM. He has designed numerous ASICs and FPGAs for Telecom Systems and he has introduced new technologies and design methodologies. He has managed the company's participation in more than 15 EU-funded research projects, with 8 in the 5G PPP and "Beyond 5G" context. Currently he is leading the research activities of the Wireless \& Network Systems BU of the company.

Idelfonso Tafur Monroy is since 2017, Professor in photonic Terahertz systems at the department of Electrical Engineering of the Eindhoven University of Technology, and since 2018 director of the Photonic Integration Technology Center (PITC). He coordinates the 5G-PPP blueSPACE project on technologies for 5G wireless systems and the ITN CELTA project with 15 PhD students working convergence of electronics and photonics technologies for applications such as THz communications, sensing and imaging. His research interests are in the area photonics technologies for Terahertz systems, converged electronic-photonic integrated circuits for applications in secure communications, sensing and computing. He is co-author of over 500 journal and conference papers and has graduated 22 PhD students. He is co-founder of the start-up Bifrost Communications on optical fiber access solutions. Prof. Tafur Monroy started his academic career in the Kharkov Polytechnic Institute in Ukraine, he received a M.Sc degree from the Bonch-Bruevitch Institute of Communications, St. Petersburg, Russia, holds a Technology Licentiate degree in telecommunications theory from the Royal Institute of Technology, Stockholm, Sweden, and a PhD degree from the Eindhoven University of Technology. He has been Professor in photonics communication technologies at Technical University of Denmark, guest Professor at the Beijing University of Post and Telecommunications, visiting scientist at the University of California at Berkeley and Fellowship Professor at the ITMO University in St Petersburg Russia, and is a senior member of IEEE.

Author details
[1] Institute for Photonic Integration, Eindhoven University of Technology, 5600 MB Eindhoven, The Netherlands. [2] Eulambia Advanced Technologies, 153 42 Agia Paraskevi, Athens, Greece. [3] Thales Research and Technology, Route Départementale, 91120 Palaiseau, France. [4] Intracom Telecom, Markopoulou Avenue, 190 02 Peania, Athens, Greece. [5] Optoscribe Ltd, Unit 1, Rosebank Technology Park, Livingston EH54 7EJ, UK.

References
1. ITU-R M.2083, IMT Vision—Framework and overall objectives of the future development of IMT for 2020 and beyond. ITU (2015)
2. J.G. Andrews, S. Buzzi, W. Choi, S.V. Hanly, A. Lozano, A.C.K. Soong, J.C. Zhang, What will 5G be? IEEE J. Sel. Areas Commun. **32**(6), 1065–1082 (2014). https://doi.org/10.1109/JSAC.2014.2328098
3. P. Rost, A. Banchs, I. Berberana, M. Breitbach, M. Doll, H. Droste, C. Mannweiler, M.A. Puente, K. Samdanis, B. Sayadi, Mobile network architecture evolution toward 5G. IEEE Commun. Mag. **54**(5), 84–91 (2016). https://doi.org/10.1109/MCOM.2016.7470940
4. A. Al-Dulaimi, Q. Ni, J. Cao, A. Gatherer, C.L. Chih-Lin, Orchestration of ultra-dense 5G networks. IEEE Commun. Mag. **56**(8), 68–69 (2018). https://doi.org/10.1109/MCOM.2018.8436048
5. J. Brenes, T.D. Lagkas, D. Klonidis, R. Muñoz, S. Rommel, G. Landi, I. Tafur Monroy, E. Grivas, E. Pikasis, G. Bernini, J.M. Fabrega, R. Vilalta, Network slicing architecture for SDM and analog-radio-over-fiber-based 5G fronthaul networks. J. Opt. Commun. Netw. **12**(4), 33–43 (2020). https://doi.org/10.1364/JOCN.381912
6. 3GPP TS 38.104, NR: Base Station (BS) radio transmission and reception. 3GPP. 3GPP Rel. 15, V15.7.0 (2019)
7. W. Feng, Y. Wang, D. Lin, N. Ge, J. Lu, S. Li, When mmWave communications meet network densification: a scalable interference coordination perspective. IEEE J. Sel. Areas Commun. **35**(7), 1459–1471 (2017). https://doi.org/10.1109/JSAC.2017.2698898

8. J. Liu, M. Sheng, L. Liu, J. Li, Network densification in 5G: From the short-range communications perspective. IEEE Commun. Mag. **55**(12), 96–102 (2017). https://doi.org/10.1109/MCOM.2017.1700487

9. T. Pfeiffer, Next generation mobile fronthaul and midhaul architectures. J. Opt. Commun. Netw. **7**(11), 38–45 (2015). https://doi.org/10.1364/JOCN.7.000B38

10. S. Rommel, D. Perez-Galacho, J.M. Fabrega, R. Muñoz, S. Sales, I. Tafur Monroy, High-capacity 5G fronthaul networks based on optical space division multiplexing. IEEE Trans. Broadcasting **65**(2), 434–443 (2019). https://doi.org/10.1109/TBC.2019.2901412

11. S. Rommel, D. Dodane, E. Grivas, B. Cimoli, J. Bourderionnet, G. Feugnet, A. Morales, E. Pikasis, C.G.H. Roeloffzen, P.W.L. van Dijk, M. Katsikis, K. Ntontin, D. Kritharidis, I. Spaleniak, P. Mitchell, M. Dubov, J. Barros Carvalho, I. Tafur Monroy, Towards a scaleable 5G fronthaul: Analog radio-over-fiber and space division multiplexing. IEEE/OSA J. Lightw. Technol. **38**(19), 5412–5422 (2020). https://doi.org/10.1109/JLT.2020.3004416

12. W. Klaus, B.J. Puttnam, R.S. Luís, J. Sakaguchi, J.M. Delgado Mendinueta, Y. Awaji, N. Wada, Advanced space division multiplexing technologies for optical networks. J. Opt. Commun. Netw. **9**(4), 1–11 (2017). https://doi.org/10.1364/JOCN.9.0000C1

13. M. Yaghubi-Namaad, A.G. Rahbar, B. Alizadeh, Adaptive modulation and flexible resource allocation in space-division- multiplexed elastic optical networks. J. Opt. Commun. Netw. **10**(3), 240–251 (2018). https://doi.org/10.1364/JOCN.10.000240

14. blueSPACE Consortium, Space Division Multiplexing 5G Fronthaul with Analog and Digital Radio-over-Fiber and Optical Beamforming—the blueSPACE Concept (2018). https://doi.org/10.5281/zenodo.1403140

15. S. Rommel, B. Cimoli, E. Grivas, D. Dodane, A. Morales, E. Pikasis, J. Bourderionnet, G. Feugnet, J. Barros Carvalho, M. Katsikis, K. Ntontin, D. Kritharidis, I. Spaleniak, P. Mitchell, M. Dubov, I. Tafur Monroy, Real-time demonstration of ARoF fronthaul for high-bandwidth mm-wave 5G NR signal transmission over multi-core fiber. in European Conference on Networks and Communications (EuCNC), Dubrovnik, Croatia (2020). p. 205–208. https://doi.org/10.1109/EuCNC48522.2020.9200921

16. A. Checko, H.L. Christensen, Y. Yan, L. Scolari, G. Kardaras, M.S. Berger, L. Dittmann, Cloud RAN for mobile networks-a technology overview. IEEE Commun. Surveys Tuts. **17**(1), 405–426 (2015). https://doi.org/10.1109/COMST.2014.2355255

17. L. Valcarenghi, K. Kondepu, P. Castoldi, Time-versus size-based CPRI in ethernet encapsulation for next generation reconfigurable fronthaul. J. Opt. Commun. Netw. **9**(9), 64–73 (2017). https://doi.org/10.1364/JOCN.9.000D64

18. L.M.P. Larsen, A. Checko, H.L. Christiansen, A survey of the functional splits proposed for 5G mobile crosshaul networks. IEEE Commun. Surveys Tuts. **21**(1), 146–172 (2019). https://doi.org/10.1109/COMST.2018.2868805

19. C. Mitsolidou, C. Vagionas, A. Mesodiakaki, P. Maniotis, G. Kalfas, C.G.H. Roeloffzen, P.W.L. van Dijk, R.M. Oldenbeuving, A. Miliou, N. Pleros, A 5G C-RAN optical fronthaul architecture for hotspot areas using OFDM-based analog IFoF waveforms. Appl. Sci. **9**(19), 4059 (2019). https://doi.org/10.3390/app9194059

20. M. Hinrichs, L.F. del Rosal, C. Kottke, V. Jungnickel, Analog vs. next-generation digital fronthaul: How to minimize optical bandwidth utilization. in *Intl. Conf. Opt. Netw. Des. Model. (ONDM)* (2017). https://doi.org/10.23919/ondm.2017.7958539

21. J. Pérez Santacruz, S. Rommel, U. Johannsen, A. Jurado-Navas, I. Tafur Monroy, Candidate waveforms for ARoF in beyond 5G. Appl. Sci. **10**(11), 3891 (2020). https://doi.org/10.3390/app10113891

22. D. Konstantinou, T.A.H. Bressner, S. Rommel, U. Johannsen, M.N. Johannson, M. Ivashina, A.B. Smolders, I. Tafur Monroy, 5G RAN architecture based on analog radio-over-fiber fronthaul over UDWDM-PON and phased array fed reflector antennas. Opt. Commun. **454**, 124464 (2020). https://doi.org/10.1016/j.optcom.2019.124464

23. S. Mosca, F. Bilotti, A. Toscano, L. Vegni, A novel design method for Blass matrix beam-forming networks. IEEE Trans. Antennas Propag. **50**(2), 225–232 (2002). https://doi.org/10.1109/8.997999

24. C. Roeloffzen, P. van Dijk, R. Oldenbeuving, C. Taddei, D. Geskus, I. Dove, R.B. Timens, J. Epping, A. Leinse, R. Heideman, Enhanced coverage though optical beamforming in fiber wireless networks. in *Intl. Conf. Transpar. Opt. Netw. (ICTON)* (2017). https://doi.org/10.1109/ICTON.2017.8025129

25. T. Nikas, E. Pikasis, S. Karabetsos, D. Syvridis, Compensation of multicore fiber skew effects for radio over fiber mmwave antenna beamforming. J. Lightw. Technol. **38**(7), 1644–1650 (2020). https://doi.org/10.1109/JLT.2019.2961557

26. F. Azendorf, A. Dochhan, K. Wilczyński, L. Szostkiewicz, P. Urban, B. Schmauss, F.J. Vilchez, L. Nadal, M.S. Moreolo, J.M. Fabrega, M. Eiselt, Characterization of multi-core fiber group delay with correlation OTDR and modulation phase shift methods. in *Opt. Fiber Commun. Conf. (OFC)* (2020). https://doi.org/10.1364/OFC.2020.M2C.5

27. Intel, Arria 10 SoC Development Kit User Guide. Intel. UG-2004 (2018)

28. Analog Devices, AD9144: Quad, 16-Bit, 2.8 GSPS, TxDAC+ Digital-to-Analog Converter. Analog Devices. Rev. C (2019)

29. Analog Devices, AD9234: 12-Bit, 1 GSPS/500 MSPS JESD204B, Dual Analog-to-Digital Converter. Analog Devices. Rev. B (2018)

30. Intel, Low Latency Ethernet 10G MAC Intel FPGA IP User Guide. Intel. UG-01144 (2018)

31. 3GPP TS 38.211, NR: Physical channels and modulation. 3GPP. 3GPP Rel. 15, V15.7.0 (2019)

32. Intel, FFT IP Core User Guide. Intel. UG-FFT (2017)

33. J.J. van de Beek, M. Sandell, P.O. Börjesson, ML estimation of time and frequency offset in OFDM systems. IEEE Trans. Signal Process. **45**(7), 1800–1805 (1997). https://doi.org/10.1109/78.599949

34. Intel, JESD204B Intel FPGA IP User Guide. Intel. UG-01142 (2019)

35. Intel, Intel Arria 10 Hard Processor System Technical Reference Manual. Intel. a10_5v4 (2019)

36. J. Yu, Z. Jia, L. Yi, Y. Su, G.-K. Chang, T. Wang, Optical millimeter-wave generation or up-conversion using external modulators. IEEE Photon. Technol. Lett. **18**(1), 265–267 (2006). https://doi.org/10.1109/LPT.2005.862006

37. W.-J. Jiang, C.-T. Lin, A. Ng'oma, P.-T. Shih, J. Chen, M. Sauer, F. Annunziata, S. Chi, Simple 14-Gb/s short-range radio-over-fiber system employing a single-electrode MZM for 60-GHz wireless applications. J. Lightw. Technol. **28**(16), 2238–2246 (2010). https://doi.org/10.1109/JLT.2010.2045341

Publisher's Note

Springer Nature remains neutral with regard to jurisdictional claims in published maps and institutional affiliations.